Modeling and Measurement of Geometrically Nonlinear Damping in a Microcantilever–Nanotube System

Bongwon Jeong,[†] Hanna Cho,[‡] Min-Feng Yu,[§,*] Alexander F. Vakakis,[†,*] Donald Michael McFarland,[⊥] and Lawrence A. Bergman[⊥]

[†]Department of Mechanical Science and Engineering, University of Illinois at Urbana—Champaign, 1206 West Green Street, Urbana, Illinois 61801, United States, [‡]Department of Mechanical Engineering, Texas Tech University, Box 41021, Lubbock, Texas 79409, United States, [§]School of Aerospace Engineering, Georgia Institute of Technology, 270 Ferst Drive, Atlanta, Georgia 30332, United States, and [⊥]Department of Aerospace Engineering, University of Illinois at Urbana—Champaign, 104 South Wright Street, Urbana, Illinois 61801, United States

ABSTRACT Nonlinear mechanical systems promise broadband resonance and instantaneous hysteretic switching that can be used for high sensitivity sensing. However, to introduce nonlinear resonances in widely used microcantilever systems, such as AFM probes, requires driving the cantilever to an amplitude that is too large for any practical applications. We introduce a novel design for a microcantilever with a strong nonlinearity at small cantilever oscillation amplitude arising from the geometrical integration of a single BN nanotube. The dynamics of the system was modeled theoretically and confirmed experimentally. The system, besides providing a practical design of a nonlinear microcantilever-based probe, demonstrates also an effective method of studying the nonlinear damping properties of the attached nanotube. Beyond the typical linear mechanical damping, the nonlinear damping contribution from the attached nanotube was found to be essential for understanding the dynamical behavior of the designed system. Experimental results obtained through laser microvibrometry validated the developed model incorporating the nonlinear damping contribution.

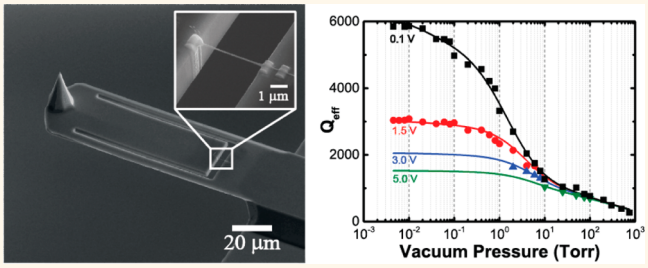

KEYWORDS: micro/nanomechanical resonator · nonlinear damping · nonlinear resonance · geometric nonlinearity · nanotubes

The advances in nanotechnology in the past decade have brought the development of various nanomechanical systems, among which nanomechanical resonators represent notable ones. Nanoresonators fabricated by integrating components such as carbon nanotubes and graphene membranes have readily shown high resonant frequency and high *Q*-factor performance owing to the nanoscale dimension, high mechanical strength and low density of the nanostructures serving as the critical mechanical elements.[1] As a result, various related devices have been developed for many applications, such as for ultrasensitive mass detection,[2−4] atom-absorption sensing,[5] and ultrahigh-frequency electrical circuitry,[6,7] as well as for the fundamental study of the quantum limit of vibration modes.[8−10]

While most of the current studies on nanomechanical resonators focus on the study of linear resonance that takes advantage of the unique mechanical and linear dynamic properties of nanowires and nanotubes, in this study we introduce a uniquely designed microcantilever system with a strong nonlinearity in the form of an attached nanotube. Although the nonlinear dynamic behavior can be conveniently realized in a micro/nanocantilever system through various physical mechanisms (*e.g.*, nonlinear electrostatic actuation), in the present work the realization of intrinsic nonlinearity in the absence of any nonlinear external potential is caused by large-amplitude oscillations of the micro/nanocantilever system beyond the regime of validity of linearly elastic response. Our aim is to develop a typical microcantilever system in dimensions and operating conditions similar to those widely used in scanning probe microscopy but with the important (and distinctive) added feature of strongly

* Address correspondence to minfeng.yu@ae.gatech.edu, avakakis@illinois.edu.

Received for review May 16, 2013 and accepted September 8, 2013.

Published online September 08, 2013
10.1021/nn402479d

© 2013 American Chemical Society

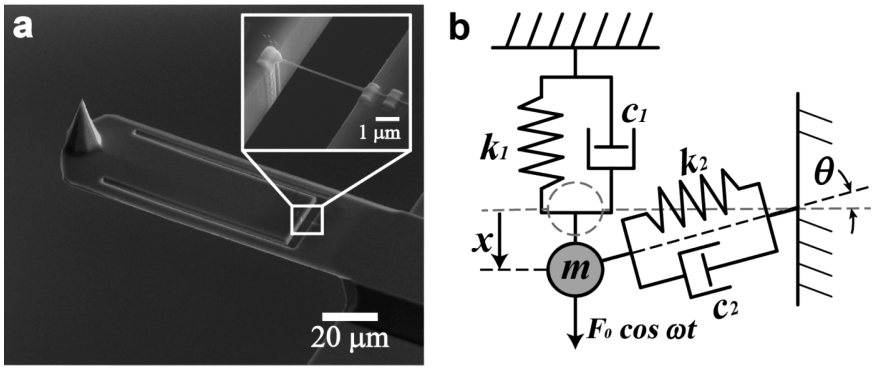

Figure 1. Fabricated nonlinear microcantilever and lumped-parameter model. (a) Scanning electron microscope image of the fabricated device. The microcantilever structure is 120 μm long, 40 μm wide and 2 μm thick, whereas the inner paddle is 75 μm long and 25 μm wide. The inset shows the attached BN nanotube, whose diameter and suspended length are 120 nm and 4 μm, respectively. (b) Simplified lumped-parameter model for the device. m denotes the effective mass of the system, and k_1 and c_1 represent the linear effective stiffness and the linear damping coefficient of the microcantilever, respectively. k_2 and c_2 are parameters arising from the nanotube attachment, standing for the axial stiffness and the viscous damping coefficient of the BN nanotube, respectively. The system is initially at the equilibrium position (denoted by a gray dashed line), and it moves by the displacement x once the system is subjected to the external force (to a configuration denoted by black dashed line). Consequently, the force acting on k_1 and c_1 changes linearly with x, whereas the vertical portion of the force acting on k_2 and c_2 changes in accordance to the relation between x and θ, resulting in nonlinearity induced by the geometrical configuration and the kinematics.

nonlinear dynamic behavior leading to broadband resonance even at relatively small drive amplitudes. Figure 1a shows the scanning electron microscope (SEM) images of the nonlinear microcantilever fabricated for incorporating significant geometrical nonlinearity. An inner paddle was carved out in a rectangular cantilever structure to create an inner cantilever having its free end close to the fixed base of the overall structure. It is expected (and later demonstrated in our modeling result) that when the microcantilever system is driven to resonate near one of its bending modal frequencies, the free end of the inner paddle can exhibit a large vertical (out-of-plane) displacement relative to the fixed base located just across a small gap. To introduce intentional strong nonlinearity, a single BN nanotube is attached across this gap as shown in the inset in Figure 1a. This local modification of the microcantilever structure alters the relation between the overall force acting on the structure and the resulting displacement, and it introduces strong geometric and kinematic nonlinearity due to the involvement of the axial stretching of the nanotube in the dynamic mechanical resonance of the system.[11,12]

In the following, we show by employing both experiment and modeling that both the geometry of the system configuration and the kinematics of the system are responsible for the nonlinear dynamic behavior of the system. We further discover that in order to account for the observed mechanical damping behavior of the system, we must include the consideration of the nonlinear damping property, beside the typical linear damping property, of the nanotube in our model development. Indeed, the geometric nonlinearity of the dynamic response amplifies the nonlinear damping associated with the tensile stretching of the nanotube, and manifests it in the overall nonlinear damping behavior of the whole system. We show that the existence of this nonlinear damping behavior, which is amplitude-dependent, results in the narrowing of the broadband resonance of this nonlinear microcantilever system. The designed microcantilever system can thus both serve as a practical nonlinear resonance system for sensing-related applications and work as a testing platform for directly studying the nonlinear damping behavior of individual nanostructures.

Modeling. Figure 1b represents the simplified, lumped-parameter model of the nonlinear microcantilever system. Considering that the microcantilever structure is geometrically large compared to the attached nanotube, the contribution of the nanotube mass to the overall mass of the system is neglected, and it is assumed that the nanotube is merely subjected to longitudinal deformation; it is noted that the nanotube is relatively soft in transverse deformation but relatively stiff in axial deformation. In the model, the vertically attached parallel spring and damper represent the microcantilever structure in its second (linear) bending mode in the absence of the nanotube attachment. The nanotube is modeled as a massless system of a linear spring in parallel with a viscous damper, which is attached horizontally between the mass and the ground. Here, the point near the base where the nanotube is anchored is modeled as the rigid ground because that point is nearly stationary. The mass moves along the x-axis, denoting the out-of-plane displacement of the free end of the inner paddle. As the mass moves in the x-direction, the magnitude of the force T exerted on the microcantilever by the horizontally attached nanotube is $T = k_2\delta + c_2\dot{\delta}$, where δ is the axial deformation of the nanotube, k_2 is the

linear stiffness, and c_2 relates to the viscous property of the nanotube. The vertical component of the force T (which represents the transverse force applied to the microcantilever), *i.e.*, T sin θ, is a function of θ as indicated in the figure. As θ is relatively small, the vertical component of the force can be expressed as T sin $\theta \approx (k_2/2L^2)x^3 + (c_2/L^2)x^2\dot{x}$, which includes a cubic term dependent on x (the amplitude) in the absence of the typical linear dependence on x that leads to the expected pure geometric nonlinearity, and a term associated with nonlinear damping originating from the viscoelastic behavior of the nanotube that leads to damping nonlinearities as we will show later. The equation of motion of the lumped-parameter model can then be expressed in the following dimensionless form (see Supporting Information Section A for the detailed derivation):

$$z'' + (2\xi_1 + \xi_3 z^2)z' + z + \alpha z^3 = q_0 \cos \Omega\tau \qquad (1)$$

Here z is the normalized vertical displacement, ξ_1 and ξ_3 are the normalized linear and nonlinear damping coefficients, respectively, and α is the normalized nonlinear stiffness coefficient. The right-hand side is the applied force, where q_0 and Ω are the normalized force and driving frequency, respectively. The approximate analytical expression for the frequency-amplitude dependence of the dynamics of eq 1 can be derived by a perturbation approach[13] and can be written as (refer to Supporting Information Sections B and D for its derivation):

$$\left[\xi_{\text{eff}}^2 + \left(\sigma - \frac{3}{8}\alpha {A_{\text{ss}}}^2\right)^2\right]{A_{\text{ss}}}^2 = \left(\frac{q_0}{2}\right)^2 \qquad (2)$$

where σ is the frequency detuning parameter (*i.e.*, $\Omega = 1 + \varepsilon\sigma$) and A_{ss} is the steady-state amplitude. Here we define an effective damping coefficient ξ_{eff} through

$$\xi_{\text{eff}} = \xi_1 + \frac{\xi_3}{8}{A_{\text{ss}}}^2 = \frac{1}{2}\left(\frac{1}{Q_0} + \frac{1}{Q_{\text{nl}}}\right) = \frac{1}{2Q_{\text{eff}}} \qquad (3)$$

where Q_0 is the Q-factor for the linear damping term, $Q_{\text{nl}}^{-1}/2$ is the damping effect contributed by the nonlinear damping effect, and $Q_{\text{eff}}^{-1}/2$ is the representative overall damping of the system. It should be noted that Q_{nl} and Q_{eff} represent the nonlinear and overall effective Q-factors, respectively, adopted from the general linear concept of Q-factor (*i.e.*, $Q_0 = 1/(2\xi_1)$), in order to obtain a better quantitative measure of the contribution of the nonlinear damping term to the overall dissipation, compared to the linear damping term which is expected to persist in the dynamics independent of the energy and pressure level. In our system, Q_0 arises from the viscous effect exerted on the microcantilever by the surrounding gaseous environment and the intrinsic damping of the beam itself, whereas Q_{nl} arises due to geometric and kinematic nonlinearities; that is, it originates from the intrinsic nonlinear damping characteristic of the attached nanotube during the oscillation.

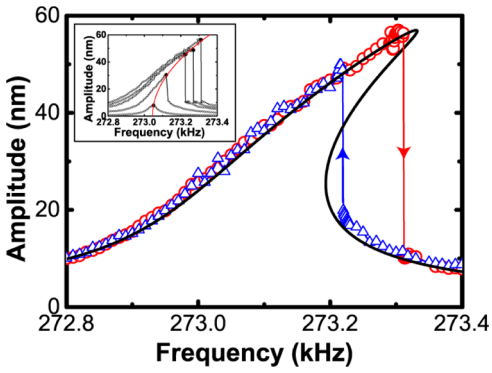

Figure 2. Nonlinear dynamical steady state response of the microcantilever with the attached BN nanotube. The frequency response spectrum is acquired with V_{pp} = 1.5 V at a vacuum pressure of 4.5 mTorr. The red circles denote data points acquired when the frequency was swept upward (forward sweep), and the blue triangles downward (backward sweep). Because of the presence of the nonlinear stiffness, the system possesses two stable branches (*i.e.*, bistability) and jump phenomena occur as shown by the blue and the red arrows, resulting in nonlinear hysteresis. The black line is the analytical solution based on the extracted α, and is fitted onto the experimental measurement to extract Q_{eff}, which is found to be 3036 ($\xi_{\text{eff}} = 1.65 \times 10^{-4}$), whereas Q_0 at V_{pp} = 0.1 V under the same vacuum pressure is 5847 ($\xi_1 = 8.55 \times 10^{-5}$). The inset shows the corresponding nonlinear resonance curves at the same pressure level, and as the excitation amplitude was set to 0.1, 0.5, 1.0, 1.25, and 1.5 V. The amplitudes at the drop frequencies are fitted by the red line (the backbone curve), resulting in $\alpha = 8.52 \times 10^{-7}$.

RESULTS

Figure 2 shows the experimentally acquired response spectrum for a microcantilever system driven with an AC excitation amplitude of 1.5 V and at a vacuum pressure P of 4.5 mTorr. Note that our initial measurement of the first two bending modes of the system revealed that the free end of the inner paddle produced greater displacement relative to the neighboring point across the gap in the second bending mode than that in the first bending mode when driven with the same V_{pp}. We thus chose the second bending mode in our study in order to involve the stronger geometric nonlinearity due to the tensile stretching of the nanotube. As seen from the acquired response spectrum, abrupt transitions are observed between the upper and lower stable branches as a result of the nonlinear hysteresis, indicating the existence of strong geometric stiffness nonlinearity induced by the nanotube attachment.

The experimentally obtained results were compared with the results from the model developed previously. The inset of Figure 2 shows the measured response curve at increasing excitation amplitude V_{pp}. With the increase of V_{pp}, the frequency band of resonant operation widens, and the drop frequency increases. The amplitude values at the drop frequency in these

response curves fit precisely into the so-called 'backbone' curve, $A_{ss} = (8\sigma/3\alpha)^{1/2}$, derived from eq 2 when all dissipative terms are set to zero and the dynamic system is Hamiltonian. The nonlinear stiffness constant α and linearized resonant frequency f_0 in eq 1 were obtained through this fitting, which gave $\alpha = 8.52 \times 10^{-7}$ and $f_0 = 273.046$ kHz. We then fit the whole response curve as shown in Figure 2a with our model result (*i.e.*, eq 2). The dimensionless force constant, q_0, was extracted from fitting the response curve acquired at an ambient pressure environment ($P = 750$ Torr), where the nonlinear damping effect was negligible, because the amplitude of oscillation of the microcantilever was small due to strong (linear) viscous damping caused by the surrounding gaseous environment and intrinsic damping; in this case q_0 is measured to be 1.88×10^{-2} at a drive amplitude of $V_{pp} = 1.5$ V. The effective damping coefficient was found to be $\xi_{eff} = 1.65 \times 10^{-4}$ ($Q_{eff} = 3036$) by fitting eq 2 to the response curve acquired at a vacuum pressure of 4.5 mTorr and at an excitation amplitude of 1.5 V (see the Supporting Information Sections C and D for the detailed description of the parameter extraction). The fitting produced response curves that matched the experimental result quite well as shown in Figure 2a.

We performed similar fitting procedures to extract the effective Q factor for a series of response curves acquired at different vacuum pressures and at different excitation amplitudes. The results are summarized in Figure 3a, in which we plot Q_{eff} as a function of the vacuum pressure under four different drive amplitudes V_{pp}. Q_0 is defined in eq 3 and represents the contribution from the linear damping (such as the hydrodynamic viscous damping and the intrinsic thermoelastic damping). Q_{nl}, as defined in eq 3, represents the contribution from the nonlinear damping and is an amplitude-dependent quantity. As expected, $Q_{nl}^{-1} \ll Q_0^{-1}$ when the device is resonating at small amplitude and the dynamic response is almost purely linear. For example, at an excitation of $V_{pp} = 0.1$ V, the maximum oscillation amplitude reaches only to around a few nanometers even at high vacuum pressure, Q_{nl}^{-1} is thus negligible, so $Q_{eff} \approx Q_0$. Q_0 as a function of the vacuum pressure acquired at a small excitation amplitude (*i.e.*, $V_{pp} = 0.1$ V) is plotted in Figure 3a. It is noteworthy that the variation of Q_0 reveals the existence of three distinct linear or nonlinear dissipation regimes for varying level of vacuum pressure. Starting from the viscously damped regime at the level of high pressure (Kn < 0.01, $P >$ ~100 Torr) where the linear dissipative effects are dominant, to the intermediate regime ($0.01 \leq$ Kn ≤ 10), and consequently transitioning to the free molecular flow regime as the vacuum pressure decreases (Kn > 10, $P <$ ~0.1 Torr).[23,24] At large excitation amplitudes (where the oscillation amplitude of the inner cantilever can reach up to around 60 nm), the effective Q-factor Q_{eff} decreases and saturates toward

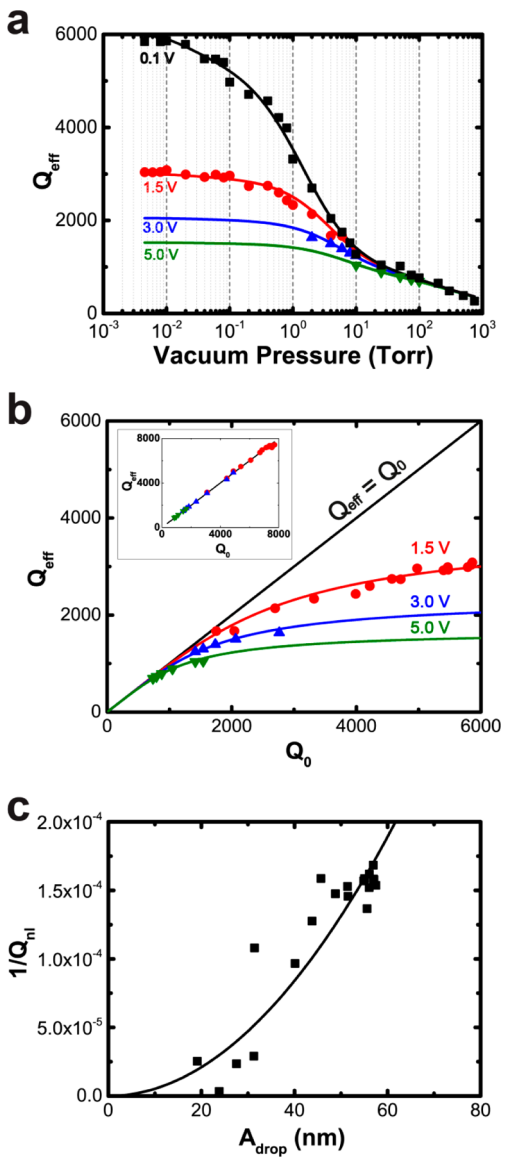

Figure 3. Nonlinear damping effect in the microcantilever with the attached BN nanotube. (a) Q_{eff} as a function of vacuum pressure. At the low excitation amplitude ($V_{pp} = 0.1$ V), a linear damping response dominates (denoted by the black line); at higher excitation amplitude, the effective Q-factor shows saturation toward higher vacuum pressure (depicted by the red, blue and green solid lines for $V_{pp} = 1.5$, 3.0 and 5.0 V, respectively), reflecting the contribution of the nonlinear damping Q_{nl}. (b) Q_{eff} plotted against the corresponding Q_0 at each vacuum pressure. (c) Q_{nl}^{-1} as a function of the corresponding oscillation amplitude at the drop frequency (A_{drop}) when $V_{pp} = 1.5$ V and the vacuum pressure is varied from 8 Torr to 4.5 mTorr.

higher vacuum pressure. This deviation of Q_{eff} from Q_0 is more clearly seen in Figure 3b, where Q_{eff} is plotted against the corresponding Q_0. For reference, we performed the same measurement on the same microcantilever without the nanotube attachment driven with the same set of excitation amplitudes under the same set of vacuum pressures. The extracted Q_{eff} is plotted against Q_0 as shown in the inset in Figure 3b, exhibiting a completely linear damping response

across the full range of the pressure and excitation amplitude variations, and showing no dependence on the oscillation amplitude as expected for a linear resonator.

The results demonstrate the critical importance of incorporating the nonlinear damping contribution into our nonlinear microcantilever resonance system. We proceed to extract the nonlinear damping coefficient ξ_3 (*i.e.*, Q_{nl}^{-1}) based on eq 3. Figure 3c shows the dependence of the extracted Q_{nl}^{-1} as a function of the amplitude at the drop frequency (A_{drop}) measured from the acquired response curves at an excitation amplitude of V_{pp} = 1.5 V and at varying vacuum pressures. Recalling that $Q_{nl}^{-1} = \xi_3 A_{ss}^2/4$ according to eq 3, ξ_3 was estimated to be 2.1×10^{-7} by fitting the measured data in Figure 3c. As ξ_3 is directly linked to c_2 which is associated with the intrinsic viscoelastic property of the nanotube, it is reasonably expected that ξ_3 is also an intrinsic property and independent of the dynamics of our microcantilever system. This is confirmed by the excellent fit in Figure 3a,b between the experimental data and the solid fitting curves obtained by assuming the same estimated value of ξ_3, even though the experimental data are acquired at varying vacuum pressures and excitation amplitudes.

The saturation of Q_{eff} toward high vacuum pressure can thus be easily understood from the consideration of the linear and nonlinear damping coexisting in our system. Toward high vacuum pressure operation, the linear damping decreases (or the energy dissipation by linear damping becomes smaller), which leads to increase of the oscillation amplitude. However, the increase of the oscillation amplitude aggravates the nonlinear damping effect through its amplitude-dependence. This counterbalance leads to the eventual saturation of Q_{eff} toward high vacuum pressures. This *Q*-factor saturation is also expected to occur in some recent studies on clamped−clamped nanoresonators,[4−10,14−22] although it was not directly reported in those studies.

The existence of nonlinear damping also affects the bandwidth of the resonance operation of our nonlinear microcantilever system. Figure 4 shows the measured drop frequency (solid symbols), which is the frequency at which the bistability transition occurs and the oscillation abruptly transits to the lower stable branch during the forward frequency sweeping, as a function of vacuum pressure at various excitation forces. We define the resonance bandwidth as $\Delta f = f_{drop} - f_0$. The analytical estimation of the drop frequency can also be derived from our model as (see Supporting Information Section E),

$$f_{drop} = f_0(1 + \alpha(\Gamma^{1/2}\xi_1 - \Gamma^{-1/2}\xi_3^{-1})^2) \qquad (4)$$

where Γ is a nominal parameter depending on ξ_1, ξ_3, and q_0. This analytical value of f_{drop} (we set $\xi_3 = 2.1 \times 10^{-7}$)

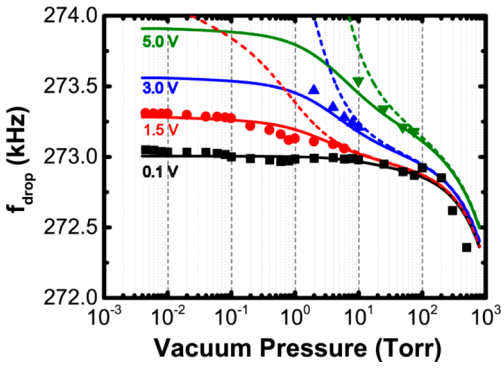

Figure 4. Drop frequency as a function of vacuum pressure. The drop frequencies (solid symbols) are measured at the points where the bistability occurs during the upward frequency sweep for the device operated at different vacuum pressure. The solid lines are fitting curves based on our nonlinear model (*i.e.*, eq 4 with $\xi_3 = 2.1 \times 10^{-7}$). The dashed lines are the corresponding model result when only the linear damping is included in the modeling.

as a function of the vacuum pressure at different excitation forces is plotted (as solid lines) in Figure 4, which again shows an excellent match with the experimental result. The dashed lines in Figure 4 represent the estimation of the drop frequency variation when only the linear damping is considered in the model analysis, in which $f_{drop} = f_0[1 + 3\alpha q_0^2/(32\xi_1^2)]$. This leads to the infinite increase of the drop frequency and thus the infinite expansion of the resonance bandwidth toward the higher vacuum pressure (*i.e.*, when $\xi_1 \rightarrow 0$) ; our experimental measurements clearly are at odds with this. We can thus obtain the upper limit of the drop frequency from eq 4 by taking $\xi_1 \rightarrow 0$, $f_{drop,max} = f_0(1 + 0.95\alpha q_0^{2/3}\xi_3^{-2/3})$, which is a finite (saturation) value as long as the nonlinear damping effect exists. This again validates the importance of the inclusion of nonlinear damping in our model consideration, especially at high vacuum pressure.

Although the nonlinear damping effect is proven to be amplitude-dependent, with the nonlinear damping force being estimated as $\xi_3 z^2 z'$ based on a viscoelastic mechanical model of the BN nanotube, it is yet still possible that there might exist other contributing factors to this nonlinear damping. As postulated by a recent study on nanotube resonators based on a single wall nanotube and graphene sheets, besides the contribution from the viscoelastic property of nanostructure itself, nonlinear phonon−phonon tunneling or friction at the clamps might also be significant factors.[25] Some studies even estimated that the contribution from the viscoelastic model can only provide a lower bound for the overall nonlinear damping effect in such resonators.[25,26] As the exact viscoelastic property of a multiwall BN nanotube during an axial deformation is not available, we instead compare the nonlinear damping coefficient extracted from our measurement with an existing value of a single wall carbon nanotube. By reversing the normalization, the

nonlinear damping coefficient c_3 ($c_3 = c_2/L^2$) is found to be 1.2×10^7 kg m^{-2} s^{-1} (see Supporting Information Section H), which turns out to be greater by 3 orders of magnitude than that of a single wall carbon nanotube, which is deduced to be 1×10^4 kg m^{-2} s^{-1} from the literature.[25] This, however, is to be expected as the multiwall BN nanotube we used in the experiment is considerably larger than a single wall nanotube, and more defective; besides, the interlayer sliding interactions might also contribute to its viscoelastic response in a significant way.[27] Nevertheless, an independent tensile dynamic study of individual BN nanotubes is clearly called for to quantify the viscoelastic properties of BN nanotubes.

CONCLUSION

In conclusion, we have introduced a practically designed microcantilever device with strong nonlinearity even at relatively small oscillation amplitudes below 100 nm operating in absence of a nonlinear external potential, and developed an analytical model with the consideration of nonlinear damping originating from the viscoelastic property of the nanotube element directly integrated into the device. Systematic experimental studies at various vacuum pressures and different excitation forces validated our analysis and demonstrated the importance of the contribution of the nonlinear damping effect on the overall dynamic behavior of this nonlinear resonance microsystem. It was found that it is the critical existence of nonlinear damping that limits the potentially unrestricted expansion of the bandwidth of the nonlinear resonance of this device toward higher vacuum pressure operation, and the saturation of both the overall effective *Q*-factor and the drop frequency at the bistable resonance branch transition. The intentionally designed nonlinear microcantilever system was also found to be a useful tool to quantitatively extract the viscoelastic properties of the individual nanowires or nanotubes integrated in the system, in this case, of an individual BN nanotube. We intend to further develop this nonlinear microcantilever system for broadband scanning probe microscopy applications.

METHODS

Device Fabrication. The nonlinear microcantilever system was fabricated by modifying a commercially available AFM cantilever (Mikro-Masch, NSC-14). The inner paddle was carved out with a focused ion beam (FIB) based machining process. A multiwalled boron nitride nanotube was then manipulated and deposited across the gap by nanomanipulation inside an SEM, and was subsequently fixed on both ends through an electron beam induced platinum deposition process.

Dynamic Response Acquisition. The fabricated microcantilever system was mounted on a small piezoelectric stack and actuated by the piezoelectric stack with an applied sinusoidal signal of amplitude V_{pp}. The dynamic response of the microcantilever system was measured by a laser vibrometer system (Polytec UHF-120) with the laser light focused on the center of the inner paddle. During the measurement, the frequency was swept up and then down to acquire the full response spectrum. To investigate the effective damping of the overall system (which, as discussed above, includes both linear and nonlinear components), the system was placed in a vacuum chamber where the vacuum pressure (P) was varied from 750 Torr down to 4.5 mTorr.

Conflict of Interest: The authors declare no competing financial interest.

Acknowledgment. The authors acknowledge the financial support of the National Science Foundation (NSF) under Grant No CMMI-100615.

Supporting Information Available: The derivation of the equation of the motion, the steady-state solution by multiple-scales analysis, the effective *Q*-factor and the drop frequency equation; the detailed explanation on the parameter extraction from the experimental measurement, the interpolation for the experimentally measured *Q*-factor and recovering the nonlinear coefficient by un-normalization, which are employed for generating Figures 2, 3, and 4. This material is available free of charge *via* the Internet at http://pubs.acs.org.

REFERENCES AND NOTES

1. Poot, M.; van der Zant, H. S. J. Mechanical Systems in the Quantum Regime. *Phys. Rep.* **2012**, *511*, 273–335.
2. Chiu, H.-Y.; Hung, P.; Postma, H. W. C.; Bockrath, M. Atomic-Scale Mass Sensing Using Carbon Nanotube Resonators. *Nano Lett.* **2008**, *8*, 4342–4346.
3. Jensen, K.; Kim, K.; Zettl, A. An Atomic-Resolution Nanomechanical Mass Sensor. *Nat. Nanotechnol.* **2008**, *3*, 533–536.
4. Cho, H.; Yu, M.-F.; Vakakis, A. F.; Bergman, L. A.; McFarland, D. M. Tunable, Broadband Nonlinear Nanomechanical Resonator. *Nano Lett.* **2010**, *10*, 1793–1798.
5. Wang, Z.; Wei, J.; Morse, P.; Dash, J. G.; Vilches, O. E.; Cobden, D. H. Phase Transitions of Adsorbed Atoms on the Surface of a Carbon Nanotube. *Science* **2010**, *327*, 552–554.
6. Jensen, K.; Weldon, J.; Garcia, H.; Zettl, A. Nanotube Radio. *Nano Lett.* **2007**, *7*, 3508–3511.
7. Gouttenoire, V.; Barois, T.; Perisanu, S.; Leclercq, J.-L.; Purcell, S. T.; Vincent, P.; Ayari, A. Digital and FM Demodulation of a Doubly Clamped Single-Walled Carbon-Nanotube Oscillator: Towards a Nanotube Cell Phone. *Small* **2010**, *6*, 1060–1065.
8. Lassagne, B.; Tarakanov, Y.; Garcia-Sanchez, D.; Bachtold, A. Coupling Mechanics to Charge Transport in Carbon Nanotubes Mechanical Resonators. *Science* **2009**, *325*, 1107–1110.
9. Steele, G. A.; Hüttel, A. K.; Witkamp, B.; Poot, M.; Meerwaldt, B.; Kouwenhoven, L. P.; van der Zant, H. S. J. Strong Coupling between Single-Electron Tunneling and Nanomechanical Motion. *Science* **2009**, *325*, 1103–1107.
10. Laird, E. A.; Pei, F.; Tang, W.; Steele, G. A.; Kouwenhoven, L. P. A High Quality Factor Carbon Nanotube Mechanical Resonator at 39 GHz. *Nano Lett.* **2011**, *12*, 193–197.
11. Anderson, D.; Starosvetsky, Y.; Vakakis, A. F.; Bergman, L. A. Dynamic Instabilities in Coupled Oscillators Induced by Geometrically Nonlinear Damping. *Nonlinear Dyn.* **2012**, *67*, 807–827.
12. Cho, H.; Jeong, B.; Yu, M.-F.; Vakakis, A. F.; McFarland, D. M.; Bergman, L. A. Nonlinear Hardening and Softening Resonances in Micromechanical Cantilever-Nanotube Systems Originated from Nanoscale Geometric Nonlinearities. *Int. J. Solids Struct.* **2012**, *49*, 2059–2065.
13. *Nonlinear Oscillations*; Nayfeh, A. H.; Mook, D. T.; Wiley: New York, 1995.
14. Sazonova, V.; Yaish, Y.; Ustünel, H.; Roundy, D.; Arias, T. A.; McEuen, P. L. A Tunable Carbon Nanotube Electromechanical Oscillator. *Nature* **2004**, *431*, 284–287.

15. Witkamp, B.; Poot, M.; van der Zant, H. S. J. Bending-Mode Vibration of a Suspended Nanotube Resonator. *Nano Lett.* **2006**, *6*, 2904–2908.
16. Garcia-Sanchez, D.; San Paulo, A.; Esplandiu, M. J.; Perez-Murano, F.; Forro, L.; Aguasca, A.; Bachtold, A. Mechanical Detection of Carbon Nanotube Resonator Vibrations. *Phys. Rev. Lett.* **2007**, *99*, 085501.
17. Bunch, J. S.; van der Zande, A. M.; Verbridge, S. S.; Frank, I. W.; Tanenbaum, D. M.; Parpia, J. M.; Craighead, H. G.; McEuen, P. L. Electromechanical Resonators from Graphene Sheets. *Science* **2007**, *315*, 490–493.
18. Garcia-Sanchez, D.; van der Zande, A. M.; San Paulo, A.; Lassagne, B.; McEuen, P. L.; Bachtold, A. Imaging Mechanical Vibrations in Suspended Graphene Sheets. *Nano Lett.* **2008**, *8*, 1399–1403.
19. Shivaraman, S.; Barton, R. A.; Yu, X.; Alden, J.; Herman, L.; Chandrashekhar, M.; Park, J.; McEuen, P. L.; Parpia, J. M.; Craighead, H. G.; *et al.* Free-Standing Epitaxial Graphene. *Nano Lett.* **2009**, *9*, 3100–3105.
20. Chen, C.; Rosenblatt, S.; Bolotin, K. I.; Kalb, W.; Kim, P.; Kymissis, I.; Stormer, H. L.; Heinz, T. F.; Hone, J. Performance of Monolayer Graphene Nanomechanical Resonators with Electrical Readout. *Nat. Nanotechnol.* **2009**, *4*, 861–867.
21. Singh, V.; Sengupta, S.; Solanki, H. S.; Dhall, R.; Allain, A.; Dhara, S.; Pant, P.; Deshmukh, M. M. Probing Thermal Expansion of Graphene and Modal Dispersion at Low-Temperature Using Graphene Nanoelectromechanical Systems Resonators. *Nanotechnology* **2010**, *21*, 165204.
22. Hüttel, A. K.; Steele, G. A.; Witkamp, B.; Poot, M.; Kouwenhoven, L. P.; van der Zant, H. S. J. Carbon Nanotubes as Ultrahigh Quality Factor Mechanical Resonators. *Nano Lett.* **2009**, *9*, 2547–2552.
23. Bhiladvala, R. B.; Wang, Z. J. Effect of Fluids on the Q Factor and Resonance Frequency of Oscillating Micrometer and Nanometer Scale Beams. *Phys. Rev. E* **2004**, *69*, 036307.
24. Verbridge, S. S.; Ilic, R.; Craighead, H. G.; Parpia, J. M. Size and Frequency Dependent Gas Damping of Nanomechanical Resonators. *Appl. Phys. Lett.* **2008**, *93*, 013101.
25. Eichler, A.; Moser, J.; Chaste, J.; Zdrojek, M.; Wilson-Rae, I.; Bachtold, A. Nonlinear Damping in Mechanical Resonators Made from Carbon Nanotubes and Graphene. *Nat. Nanotechnol.* **2011**, *6*, 339–342.
26. Zaitsev, S.; Shtempluck, O.; Buks, E.; Gottlieb, O. Nonlinear Damping in a Micromechanical Oscillator. *Nonlinear Dyn.* **2012**, *67*, 859–883.
27. Sawaya, S.; Arie, T.; Akita, S. Diameter-Dependent Dissipation of Vibration Energy of Cantilevered Multiwall Carbon Nanotubes. *Nanotechnology* **2011**, *22*, 165702.